Rock Mech Rock Eng (2014) 47:2287–2298
DOI 10.1007/s00603-013-0499-z

TECHNICAL NOTE

Mechanical Model for Predicting Closure Behavior of Rock Joints Under Normal Stress

Zhi-Cheng Tang · Quan-Sheng Liu · Cai-Chu Xia · Ying-Long Song · Ji-Hui Huang · Chun-Bo Wang

Received: 15 July 2013 / Accepted: 24 October 2013 / Published online: 13 November 2013

Keywords Rock joint · Closure deformation · Morphology · Waviness component · Unevenness component

List of Symbols

a	Radius of a circular contact area
a_h	Height of asperity in Fig. 11
a_0	Coefficients of Fourier series in Eq. (1)
a_m	Coefficients of Fourier series in Eq. (1)
b_m	Coefficients of Fourier series in Eq. (1)
b	Radius of a special curve in Eq. (6)
c	Constant
d	Distance between the two reference surfaces after loading
d_0	Distance between the two reference surfaces before loading
E	Young's modulus of rock
E_a	Modulus of asperity
E_b	Modulus of bulk material
E'	$E/2(1-\upsilon^2)$
e_0	Initial aperture
F	External force being exerted on one asperity in Fig. 11
$f(z)$	Height distribution function of the asperities with the topographical height z as the independent variable
$G(m)$	Normalized amplitude of the waviness
g	Generalized function
h,	Integers and independent variables
i,	Integers and independent variables
m,	Integers and independent variables
n	Integers and independent variables
JRC	Joint roughness coefficient
k	Composite spring constant between asperity and bulk substrate
k_a	Asperity spring constant
k_b	Bulk substrate spring constant
N	Total number of sampling data in Eq. (1)
P	External force being exerted on one peak of the waviness
p_0	Maximum contact pressure
$q_1(r)$	Distribution function of the compressive contact stress
$q_2(r)$	Distribution function of the compressive contact stress
$q_3(r)$	Distribution function of the compressive contact stress
R	Curvature radius of the waviness
r	Distance from the contact center
r_a	Radius of contact region in Fig. 11
r_b	Radius of circular contact region on top of bulk substrate in Fig. 11
U_z	Normal displacement of the contact surface
$u(r)$	Asperity deformation in Eq. (7)
$w(r)$	Deformation of waviness
z	General topographical heights
$z(i)$	The ith measured topographical height

Z.-C. Tang (✉) · Q.-S. Liu
School of Civil and Architectural Engineering, Wuhan University, Wuhan 430072, People's Republic of China
e-mail: tangzhichengok@126.com

Z.-C. Tang · C.-C. Xia · J.-H. Huang · C.-B. Wang
Department of Geotechnical Engineering, College of Civil Engineering, Tongji University, Shanghai 200092, People's Republic of China

Y.-L. Song
Hunan Provincial Electric Power Design Institute, Changsha 410007, People's Republic of China

$z_c(i)$	The ith topographical height of composite topography
z_{upper}	Topographical heights of the upper surfaces of a joint
z_{lower}	Topographical heights of the lower surfaces of a joint
Δ	Sampling interval
υ	Passion's ration
β	Root mean square radius of peak
η	Mean peak density of unevenness in composite topography of a joint
$\varepsilon_r(i)$, $\varepsilon_h(i)$	Random component of surface topography in Eqs. (1), (3)
φ	The angle shown in Fig. 4
φ_h	Amplitude angle of waviness
ρ	Asperity radius in Fig. 11
δ	Normal displacement in Fig. 11
δ_a	Asperity deformation in Fig. 11
δ_b	Bulk substrate deformation in Fig. 11
σ_n	Normal stress

1 Introduction

The mechanical properties of rock mass are mainly governed by the joints which it contains. As a consequence, over the past decades, many researchers have focused on the mechanical properties of rock joints and numerous applications could benefit from this, such as geo-thermy, petroleum reservoirs, as well as underground disposal of high-level radioactive wastes and CO_2. This paper focuses on the closure deformation of rock joints under compressive loading and this is the first step in the direction of a more global hydro-mechanical study of joint. Many models have been developed to describe the mechanical behavior of a joint under normal stress and which can be classified into three categories: empirical model, numerical model, and theoretical model.

In the study of joint deformability, it has been generally observed that the relation between closure deformation and the normal stress is non-linear. Many empirical models are proposed to fit the experimental data by using non-linear mathematical function. Goodman (1976) suggested hyperbolic relation to describe joint closure under normal compressive stress. Bandis et al. (1983) and Barton et al. (1985) presented a modification of Goodman's hyperbolic model which was shown to provide a better fit to experimental data across the whole range of stress and closure values, known as BB model. BB model established a relationship between JRC and mechanical parameters such as maximum closure of the fracture and normal stiffness, which are used mostly in practice (Bower and Zyvoloski 1997; Guvanasen and Chan 2000; Itasca Consulting Group 2004; Baghbanan and Jing 2007; Tao et al. 2011; Zhao et al. 2011; etc.). However, such a model makes use of parameters obtained from experimental data only, therefore there may be difficult for being extend to general behaviors of rock joints. A power-law model for joint closure was given by Swan (1983) which provides a good fit to experimental data only at low stress levels. The power-law model also suggests infinite initial fracture compliance, which may be appropriate only for some highly compliant rock joints. Malama and Kulatilake (2003) presented a generalized exponential model to predict joint deformation behavior under normal compressive loading. Nevertheless, all of these empirical models cannot be used to predict the closure deformation of rock joints because of the non-predictive nature.

Several numerical models, asperities represented by cylinders, can take into account both asperity deformations and deformations of the rock surrounding the asperities (Cook 1992; Hopkins 2000; Lee and Harrison 2001; Marache et al. 2008). These models rely on an accurate description of the topography of joint and of the void space. Superposition principle is used and the total closure deformation is the sum of three parts: deformation of the asperity itself due to the forces acting directly on it, deformation of the bulk material surrounding the asperity due to the forces acting on the asperity, and deformation of the bulk material results in mechanical interaction between contact zones. For a given joint, it is required to develop a special computation program. Because of the lake of versatility, this class of models is inconvenient to use.

Theoretical models (Greenwood and Williamson 1966; Greenwood and Tripp 1970; Yamada et al. 1978; Swan 1983; Brown and Scholz 1985, 1986), based on the Hertz contact theory, can be used to predict the closure deformation of joint under normal stress. But most of the theoretical models used only the unevenness to describe the joint surface and did not consider the contact state cases between two rough surfaces (Xia et al. 2003). According to ISRM (1978), joint topography is made up of large-scale waviness component and small-scale unevenness component. Both of them have different effect on the closure deformation (Xia et al. 2003). A mathematical method was given by Xia et al. (2003) to identify the two components and joint was classified into three contact state cases according to the waviness and unevenness components. A general load-closure model was proposed by Xia et al. (2003). Xia's model can take into account the effects of both the waviness and unevenness components and also the contact state cases.

The above theoretical models give us a relative correct understanding of joint closure behavior under normal

stress, however, they ignored the substrate deformation caused by asperity deformation and the interaction between asperities which have great influence on the hydro-mechanical behavior of rock joints. On the basis of Xia model, we present an improved model capable of predicting closure deformation of rock joints. Both surface topography (waviness component and unevenness component) and substrate deformation caused by asperity deformation can be taken into account by the new model. Several experiments are performed to validate the proposed model.

2 Description of Joint Surface

2.1 Method to Separate Waviness and Unevenness Components

The method to identify and separate the waviness and random unevenness components for rock joints is proposed by Xia et al. (2003) presented in the ensuing.

If surface topography of joint contains determinate waviness component, the data order array $z(i)$ with the total number N gained by measuring surface topography can be expressed by the following Fourier series:

$$z(i) = \frac{a_0}{2} + \sum_{m=1}^{N} \left[a_m \cos\left(\frac{2\pi mi}{N}\right) + b_m \sin\left(\frac{2\pi mi}{N}\right) \right] + \varepsilon_r(i) \tag{1}$$

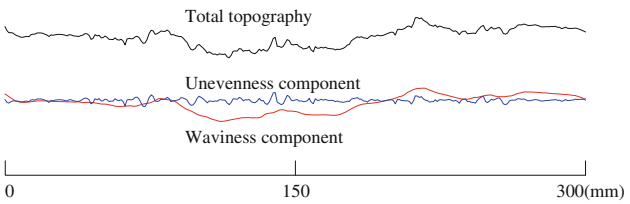

Fig. 1 Total topography and the two components

where, $a_0 = \frac{2}{N}\sum_{i=1}^{N} x(i)$; $a_m = \frac{2}{N}\sum_{i=1}^{N} x(i)\cos\left(\frac{2\pi mi}{N}\right)$; $b_m = \frac{2}{N}\sum_{i=1}^{N} x(i)\sin\left(\frac{2\pi mi}{N}\right)$.

The amplitude of each waviness is $c_m = \sqrt{a_m^2 + b_m^2}$ and its normalized value is defined as $G(m) = \frac{c_m^2}{\sum_{i=1}^{n} c_i^2}$.

If there is a waviness component $m = h$ in the surface topography of a rock joint according to measurement, the Eq. (1) is expressed as

$$z(i) = a_h \cos\left(\frac{2\pi mi}{N}\right) + b_h \sin\left(\frac{2\pi mi}{N}\right) + \varepsilon_h(i) \tag{2}$$

The random unevenness component of this surface topography is expressed as

$$\varepsilon_h(i) = z(i) - c_h \cos\left(\frac{2\pi hi}{N} + \varphi_h\right) \tag{3}$$

A typical composite profile with waviness and its waviness and unevenness components by using above method to identify and separate are shown in Fig. 1.

2.2 Composite Topography

According to Brown and Scholz (1985), the composite topography of a joint is obtained by summing coordinates of its upper and lower surface profiles, shown in Fig. 2. The upper surface height at the lateral coordinate point i is added to the lower surface height at the lateral coordinate point $i + m$, where the lateral shift interval m indicates the contact states for the composite topography of a joint, i.e.,

$$z(i) = z_{\text{upper}}(i) + z_{\text{lower}}(i + m) \tag{4}$$

For perfect matched joints, the composite topography $z(i)$ represents a straight line and the composite topographic can be expressed by

$$z(i) = z_{\text{upper}}(i) + z_{\text{lower}}(i) = d_0 = \text{cost}. \tag{5}$$

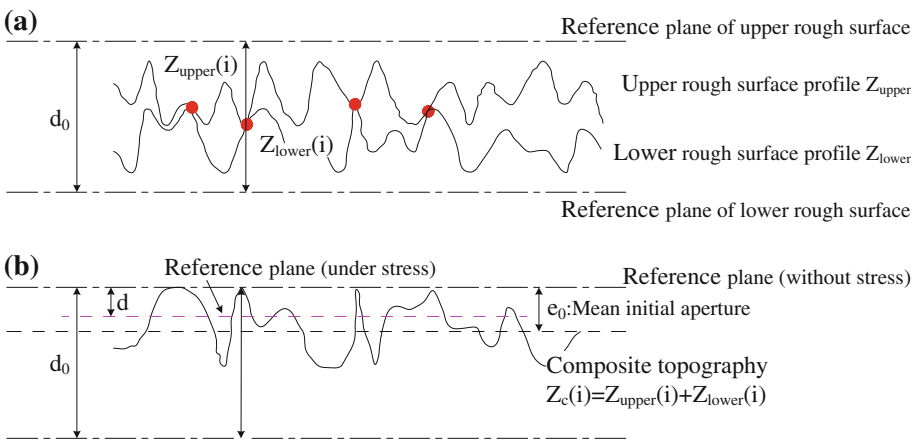

Fig. 2 Sketch of two rough surface profiles of a joint and the associated composite topography (Cook 1992)

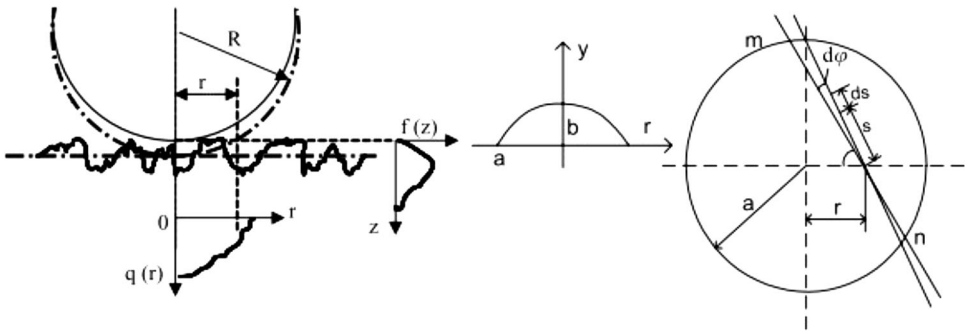

Fig. 3 Simplified model for the contact between waviness surface and unevenness surface of the composite topography for a rock joint (Xia et al. 2003)

2.3 Contact States of Rock Joints

According to both the upper and lower joint surface and its associated composite topography, the contact state of joint can be classified into the following three cases (Xia et al. 2003):

- *Case 1*: the two surface profiles of joint contain only the random unevenness and the composite topography still contains only the random unevenness.
- *Case 2*: the two surface profiles of a joint contain the waviness components whilst the composite topography contains only the random unevenness.
- *Case 3:* the two surface profiles of a joint contain waviness components and random unevenness components. The waviness components are uncorrelated. The composite topography then contains both the waviness component and the random unevenness components.

3 Closure Deformation Model

As shown in Fig. 3, Xia et al. (2003) assume the distribution of compressive contact pressure, $q_1(r)$, at the contact area is

$$q_1(r) = \frac{P}{\pi c}\left(\frac{1}{r^2+4b^2} - \frac{1}{a^2+4b^2}\right) \tag{6}$$

where, $c = \ln\left(\frac{a^2+4b^2}{4b^2}\right) - \frac{a^2}{a^2+4b^2}$

As the pressure distribution of asperity contact is relevant to the asperity deformation $u(r)$, another equation for the distribution of the compression pressure at the contact area can be obtained as follows according to the Brown model (Brown and Scholz 1985, 1986) [for detailed derivation of Eqs. (8) and (9), see Xia et al. (2003)]

$$q_2(r) = \frac{4}{3}E'\eta\sqrt{\beta}\int_0^{u(r)}\sqrt{[u(r)-z]^3}f(z)\mathrm{d}z \tag{7}$$

$$u(r) = \frac{a^2-r^2}{2R} + w(a) - w(r) \tag{8}$$

$$w(r) = \frac{2P}{\pi^2 E' bc}\int_0^{\pi/2}\left[\arctan\left(\frac{1}{2b}\sqrt{a^2-r^2\sin^2\varphi}\right) - \frac{2b}{a^2+4b^2}\sqrt{a^2-r^2\sin^2\varphi}\right]\mathrm{d}\varphi \tag{9}$$

On the basis of Eq. (7), if we take into account the substrate deformation caused by the asperity deformation, the contact pressure can be expressed as (see "Appendix" for detailed derivation):

$$q_3(r) = \frac{4}{3}E'\eta\sqrt{\beta}\int_0^{u(r)}\sqrt{\{g[u(r)-z]\}^3}f(z)\mathrm{d}z \tag{10}$$

For solving this model, the initial values of a, b shall be given (nonzero value), and then the distribution of compression stress $q_1(r)$ can be calculated by Eq. (6). The deformation of the waviness $w(r)$ and $w(a)$ are calculated from Eq. (9). The asperity deformation $u(r)$ is calculated from Eq. (8). Another distribution of the compression stress $q_3(r)$ is obtained by substituting $u(r)$ into Eq. (10). The procedure above is repeated until the two distributions of the compression pressure $q_1(r)$ and $q_3(r)$ are equal at $r = 0$ and $r = 0.5a$. Figure 4 outlines the calculation algorithm of the proposed mathematical model.

When the closure deformation curves are calculated by using the above closure deformation model, the data of surface topography of the joint should be treated and calculated as follows (Xia et al. 2003):

- Calculate the composite topography of a joint from the test data of surface topography and the contact states of the two surfaces of the joint.
- Test and distinguish the waviness component in the composite topography of the joint.
- Calculate the topographical parameters of the waviness and unevenness components in the composite topography of the joint. The topographical data must be processed through the zero average before calculating the topographical parameters.

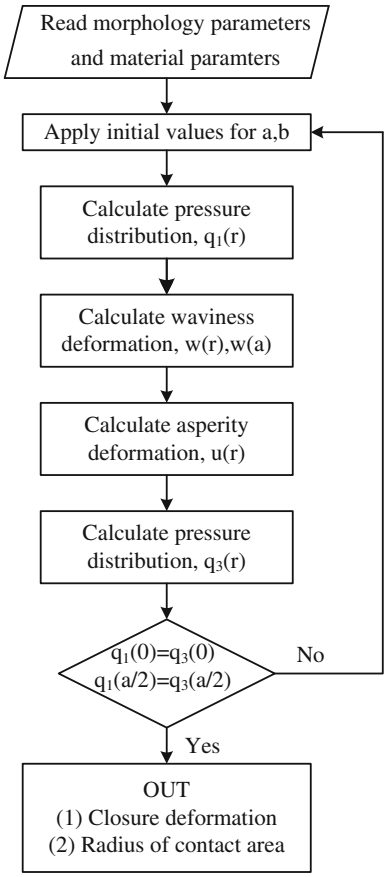

Fig. 4 Algorithm for the new mathematical model

If there is no waviness component in the composite topography of a joint, the general model for Case 3 will automatically degenerate into the contact closure deformation model between a smooth surface and a random rough surface. This degenerated contact corresponds to Cases 1 and 2. The general model is also applicable to Cases 1 and 2 if the curvature radius of waviness is zero.

The closure deformation of a joint is determined by the waviness and unevenness components of the composite topography for a specific contact state. The closure deformation models applicable to the three cases are summarized in Table 1. Compared with other models, the proposed can take into account the substrate deformation and also the effect of morphology components.

4 Experiments and Validation

4.1 Sample Preparation

The used samples have been prepared from gray granite whose average grain size is about 3.5 mm, known as quasi-isotropic granite. We have cut samples with dimensions $300 \times 300 \times 150$ mm from blocks of this granite. The joints were obtained by rupture according to three points bending method. During this operation the joint surfaces were maintained by silicon rubber for saving the quality of the surface at the instant of the failure. We established marks for these samples of rock joints based on the direction of the mean plane of rupture, and on the regularity of their roughness in order to be able to choose the most interesting rock joint surfaces to carry out tests with high quality. We extracted two joints from this series. Then, we made samples as replicas of the two rock joints. In order to be able to carry out several tests on identical surfaces of joints (geometry and mechanical properties), we decided to work on replicas in mortar of our models.

The model material is a mixture of plaster, sand, and water at the ratio of 3:2:1 (weight). All the samples were cured at a constant temperature of 25 °C in a chamber for about 28 days. The uniaxial compressive strength and density of several cubic concrete replicas with diameter 50 mm and height 100 mm were measured in the laboratory, which gave an average value of 27.5 MPa and density of 2,200 kg/m^3. The Young's modulus of the model material is 6.1 GPa and Poisson's ratio is 0.16.

Table 1 Three contact cases of joint and its suitable model

Case	Topographical characteristics of joint surface	Suitable model	Type of input parameters for solving
1	The topographies of the two surfaces of a joint are random unevenness, and their composite topography is still random unevenness	New model and Xia model ($R \to \infty$)	Composite parameters of surface topographies of a joint
		Brown model	Parameters of composite topography of a joint
		Greenwood model	Parameters of surface topographies of a joint
		Yamada model and Swan model	Profile data of surface topographies of a joint
2	The topographies of the two surfaces of a joint contain waviness, and their composite topography is still random unevenness	New model and Xia model ($R \to \infty$)	Parameters of composite topography of a joint
3	The topographies of the two surfaces of a joint contain waviness, and their composite topography still contains tendency waviness too	New model and Xia model (R is limit)	Parameters of composite topography of a joint

According to the single surface topography, the samples are divided into two groups, named Group I, II, and each group consists of four samples with the same morphology.

4.2 Measurement System

Rock joint surface were measured using a 3D stereo-topometric measurement system developed by Xia et al. (2008, 2013). Such a system has the advantages of high precision and good repeatability, as well as being fast and easy to use since it is able to digitize the entire surface at once. The system works on a novel principle compared to one-camera fringe projection sensors and consists of a measurement head containing a central projector unit and two CCD cameras with the resolution of 1.44×10^6 pixel. Various white-light fringe patterns are projected onto the object surface and recorded by two digital cameras, which are integrated into the measurement head, from two different angles (Fig. 5). Due to the high data density resulting from the optical measurement process, details of the rough surface can be captured precisely. Depending on the selected camera shutter speeds, one measurement requires 5–15 s to be completed. 3D coordinates are computed independently with high accuracy for each of the camera pixels. The resolution of the spatial location of each point in the 3D space (point cloud) along x, y, z direction is ± 20 μm. In this work, point spacing is selected as 0.3 mm when reconstruct joint surface. The surface spatial variations of joint specimens are shown in Fig. 6.

The basis of the surface point triangulation is the interior and exterior orientation of the sensor elements, which must be determined by a special calibration procedure. The calibration procedure relies on the fact that the parameters of a mathematical model describing the camera operation can be extracted from target locations. The calibration object consists of a plane with circular targets whose coordinates need not be known exactly. They are simultaneously calculated by a bundle adjustment light. Only the distance between two points of the calibration object should be known a priori to determine the scale of the coordinates. In the laboratory, the calibration accuracy of this system is usually 0.002 mm.

4.3 Test Procedure

Joint surface topography and contact states between the upper and the lower joint surfaces have a dominant effect on its closure deformation (Xia et al. 2003). We can obtain joints with different contact states by using different dislocations between the upper and lower joint surface profiles. In this work, the amount of lateral dislocation was 5, 10, or 15 mm, respectively. Each combined joint set can be considered as an individual joint with its own composite topography. The eight sets of combined joints were used in

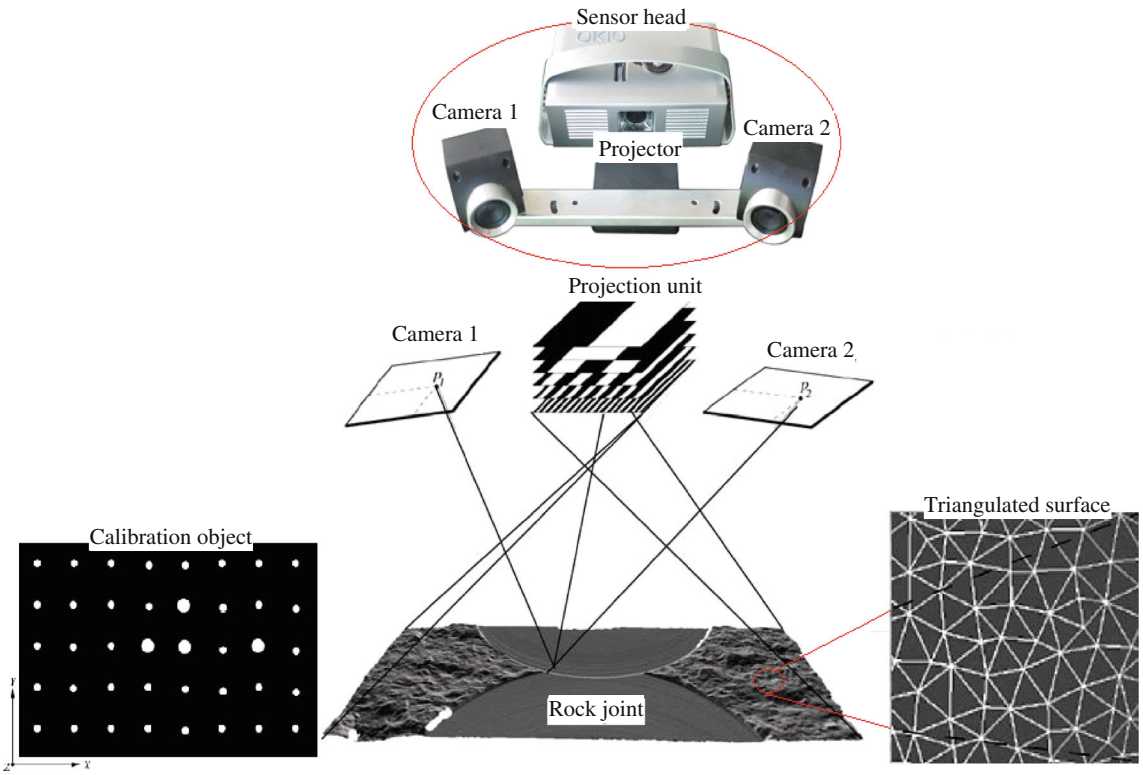

Fig. 5 Stereo-topometric scanner used to digitize surface roughness (Xia et al. 2013)

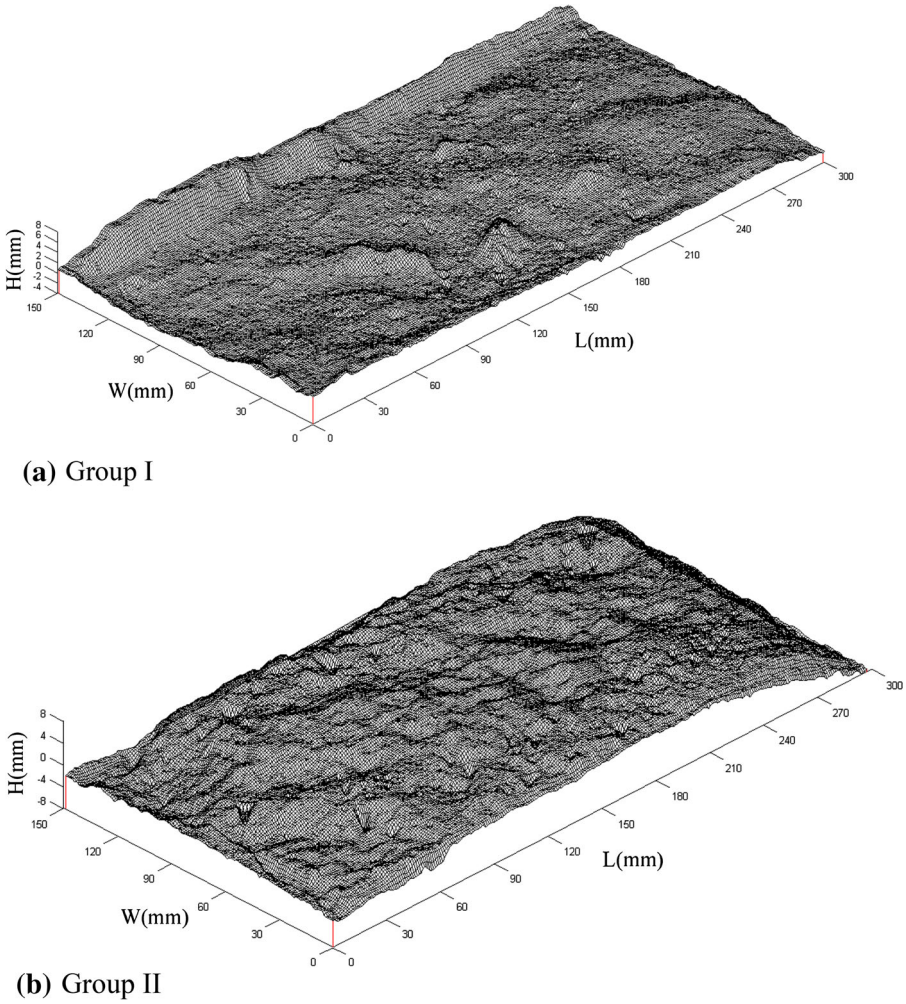

Fig. 6 Spatial variation of the bottom surfaces of the respective joint specimens

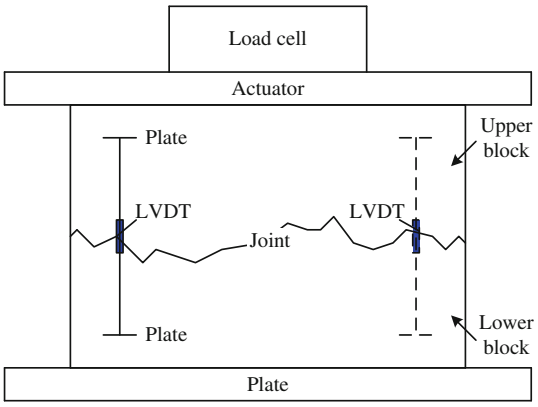

Fig. 7 The schematic of closure deformation measurement by LVDT

the closure testing. We used the following approach to impose the lateral dislocation between the upper and lower surfaces (Xia et al. 2003):

- Initially, the entire upper sample block and the lower sample block are placed tightly together as one single man-made joint.
- Under this completely mated joint state, a set of scale lines are drawn at 1 mm intervals on the two symmetric surfaces of the joint plane.
- The lower block sample is then fixed.
- The upper block is then moved slowly to make lateral dislocations of 5, 10, or 15 mm, respectively, along the scale lines.

The closure tests were carried out on a servo-controlled testing machine, at Rock Mechanics and Engineering Center of Tongji University. The specimens were pre-loaded by 50.0 kPa to stabilize the testing system and normal stress was increased at a rate of 0.002 MPa/s until to a designated value, 3.0 MPa. The normal displacement was measured by LVDT with an accuracy of ± 1 μm, which was connected to a digital data acquisition system with an adjustable data-recording rate. Two pieces of plates bearing extensometers were installed on the two symmetric surfaces of the lower sample part. Two pieces of plates transmitting displacement were stalled on the two symmetric surfaces of the upper sample part (Fig. 7). They were made with angle steel with large stiffness. The

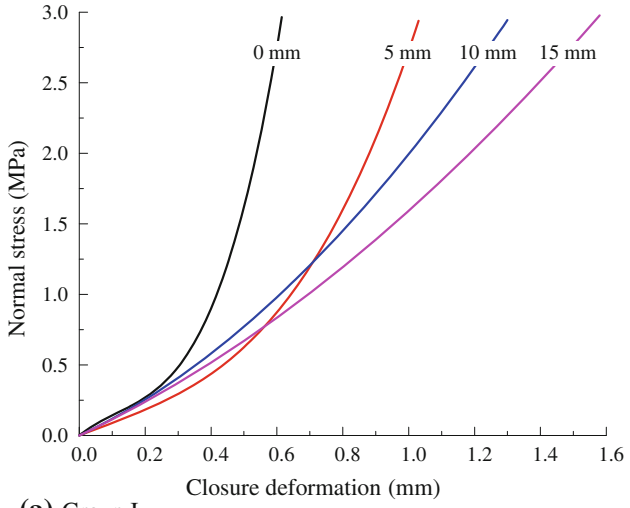

(a) Group I

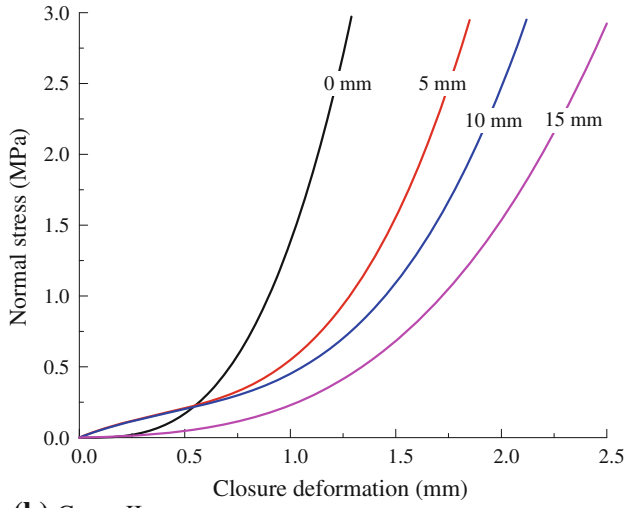

(b) Group II

Fig. 8 Results of joint closure-deformation curves under different contact state

relative displacements between the plates bearing and plates transmitting displacement under different compressive loads were measured with two clip-type extensometers. The average value of the two extensometers subtracting the deformation of the intact rock between two pre-determined signs under the corresponding axial load was considered to be the joint closure deformation.

4.4 Analysis and Validity of the Experimental Results

Each test has been made twice, so it becomes possible to evaluate the repeatability of the mechanical behaviors. Results of the compression tests are presented in Fig. 8. The curves of mean normal relative displacement versus normal stress have nearly the same shape, and have been described by many authors, such as Goodman (1976) and Bandis et al. (1983). The closure curves possess a high degree of non-linearity. As the normal stress increases, the curves gradually approach a vertical line that corresponds to the maximal joint closure deformation. We can also know that the closure curves for one joint with different contact depict substantial variations. The larger the dislocation between the two joint surfaces, the more the difference among the load-closure curves. This result indicates that joint closure behavior has a substantial dependence on the characteristics of composite topography under a specific contact state.

The material and morphology parameters used for predicting closure deformation of joints are given in Table 2. A comparison between the test and the calculated closure deformation are shown in Figs. 9 and 10. Compared to Xia model, the calculated curves by the new model are closer to the experimental. Errors associated with topography measurement and initial aperture estimation may be the reasons for the difference between the theoretic curve of the new model and the experimental curve. Another factor may be the used morphology parameters which are scale and size dependent. During the laboratory testing, we tried to obtain joint samples with contact state Case 2. However, we were failure to obtain such joint samples for testing. Hence, experimental verification of the new model for Case 2 should be carried out in future studies.

How a joint deforms under stress depends on its physical attributes, including the roughness of the joint surfaces, the spatial geometry of the contact area and topographical features (Hopkins 2000). As for a real rock joint, surface roughness is directional dependent, so we will obtain different composite topography and varied closure deformation when the lateral dislocation forwards different direction. Greenwood model cannot reflect this feature and the calculated closure deformation is unique as long as the single surface of joint is the same. As for

Table 2 Input parameters for validity of the proposed models

Dislocation (mm)	Group I				Group II			
	η (mm^{-2})	β (mm)	e_0	R	η (mm^{-2})	β (mm)	e_0	R
5	0.1666	6.3248	1.36	∞	0.0970	5.1626	2.18	141.8
10	0.1727	6.2276	1.93	∞	0.0950	5.4584	2.66	144.3
15	0.1738	6.443	2.24	∞	0.0955	5.3642	3.02	143.7

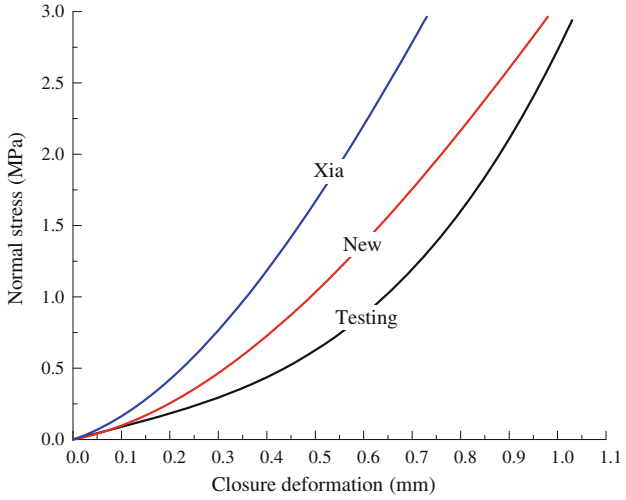

(a) dislocation of 5 mm

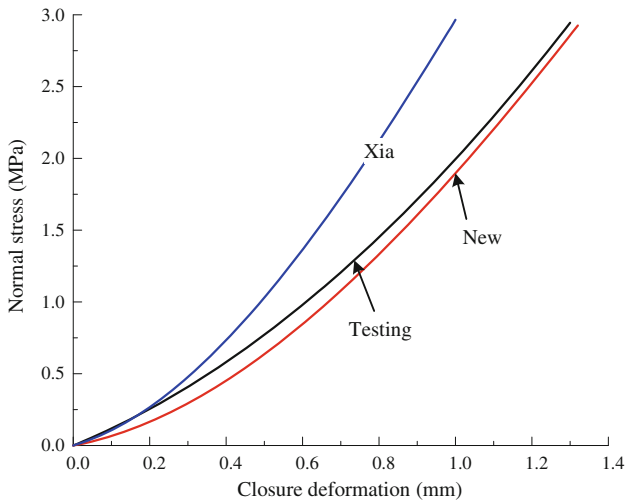

(b) dislocation of 10 mm

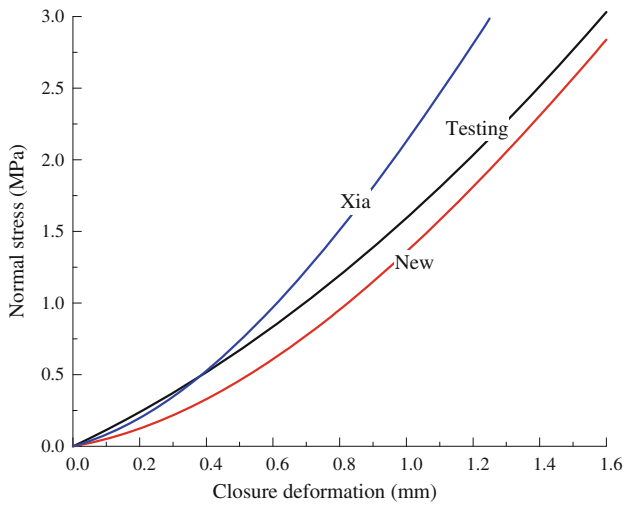

(c) dislocation of 15 mm

Fig. 9 Comparison between the experimental and theoretical closure deformation curves for Group I

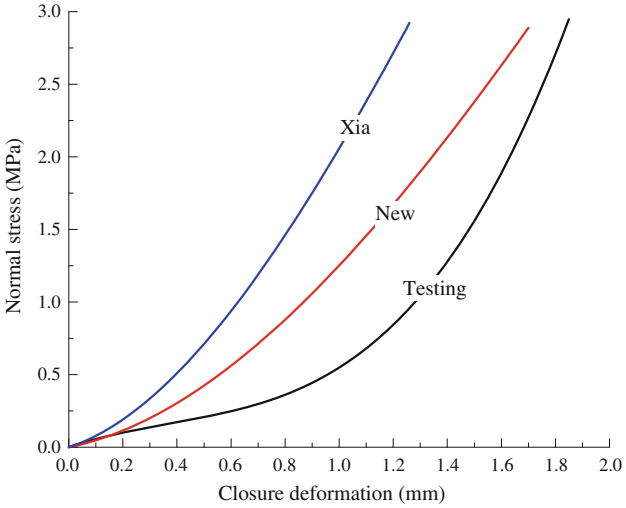

(a) dislocation of 5 mm

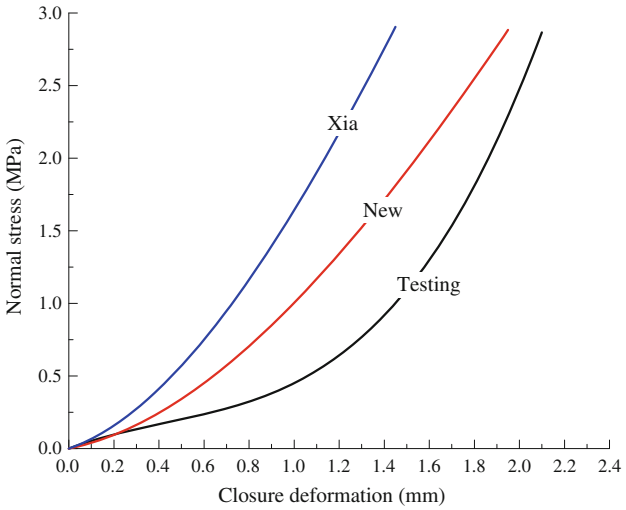

(b) dislocation of 10 mm

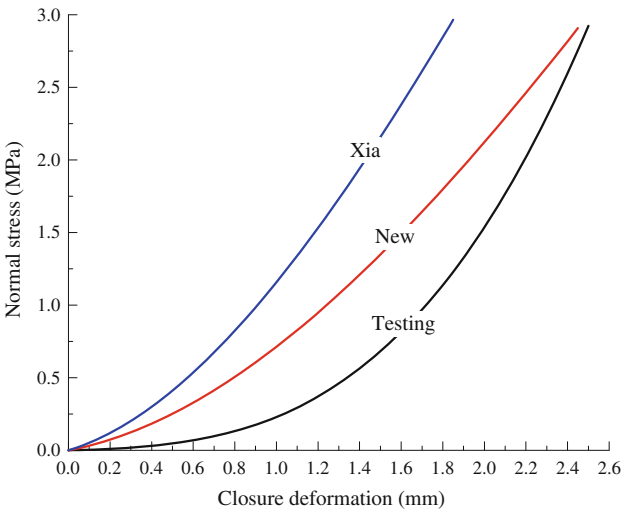

(c) dislocation of 15 mm

Fig. 10 Comparison between the experimental and theoretical closure deformation curves for Group II

the Xia model and the proposed model, we will obtain different closure deformation when the composite topography changed. For a realistic closure process, roughness and waviness evolve with the deformation, which means that the friction between two surfaces changes gradually. Actually, the changing contact friction can be reflected by the increasing normal stiffness during the process of closure. Compared with the Xia model, the calculated stiffness by the present model is smaller and this would be expressed by the contact model using two springs in series.

Deformation of the bulk material surrounding the joint results in mechanical interaction among contacting asperities and changes in the geometry of the void space between the joint surfaces and these results have significant implications for almost any endeavor in fractured rock, including predicting the hydro-mechanical response of a rock mass to changes in stress, understanding deformation and failure of joints under shear stress (Hopkins 2000). However, there is no effort to discuss the interaction between asperities because of its complexity and, this is our future work.

5 Conclusions

Many factors influence the closure deformation of rock joints and we pay more attention to the effect of its roughness. Other factors, such as substrate deformation, usually have been ignored or at least not straight forward to be expressed in the existed theoretical models. Compared to other models, Xia model is the only one which can take into account the different effect of components (waviness component and unevenness component) to joint closure deformation. According to elastic analysis for single asperity, two springs in series concept was used and the realistic deformation of asperity was derived on basis of deformation compatibility conditions. The substrate deformation has great effect on joint deformation. Then, we estimate the closure deformation of joints under normal stress by improvement of Xia model to account this substrate deformation. The proposed model can account the effect of both surface components and substrate deformation. Several closure tests are performed to validate the proposed model and the prediction compares well with the experiment results.

Acknowledgments The work is supported by National Natural Science Foundation of China under projects 41130742 and Major State Basic Research Development Program of China (973 Program, No. 2014CB046904). The main research work was done by the first author during the course of studying for the Ph.D degree at Tongji University, supported by National Natural Science Foundation of China under project 40972178. The authors acknowledge the anonymous reviewer for the critical reviews and constructive comments that lead to significant improvements to the manuscript.

Appendix

Single asperity and bulk substrate were analyzed separately according to elastic analysis using two springs in series concept as shown schematically in Fig. 11. The realistic contact pressure on the substrate is more complicated depending on the geometrical and physical properties of asperity and substrate.

According to Hertz theory, the stiffness of an asperity is given by (Popov 2010)

$$k_a = \frac{\mathrm{d}F}{\mathrm{d}\delta_\mathrm{a}} = 2\sqrt{\rho}E_\mathrm{a}\sqrt{\delta_\mathrm{a}} \tag{A1}$$

In the case of bulk substrate, a Hertz pressure instead of a constant pressure was used to model the substrate stiffness. When the Hertz pressure is applied to a circular region with a radius of r_b in the elastic half-space, according to elastic analysis, the normal displacement of the surface could be obtained by (Popov 2010)

$$U_z(r) = \frac{\pi p_0}{4E_\mathrm{b}r_\mathrm{b}}\left(2r_\mathrm{b}^2 - r^2\right) \quad 0 \le r \le r_\mathrm{b} \tag{A2}$$

$$p_0 = \frac{3}{2}\frac{F}{\pi r_\mathrm{b}^2} \tag{A3}$$

The normal displacement at the centre of the circular region could be expressed as

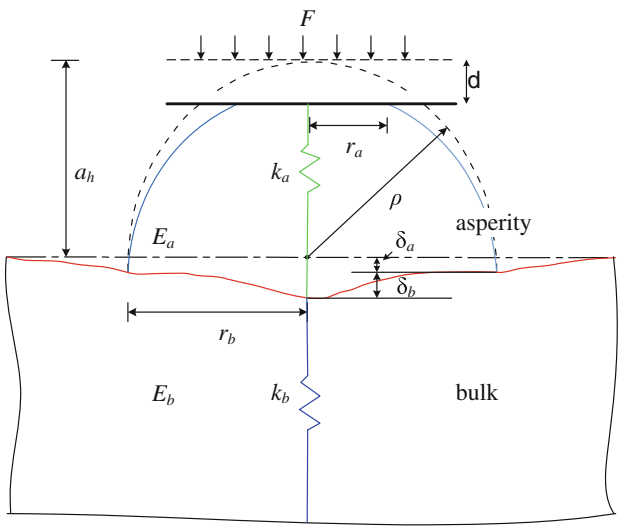

Fig. 11 Single asperity contact-deformation model (Modified from Yeo et al. 2009)

$$\delta_b = U_z(0) = \frac{\pi p_0}{2E_b} r_b \tag{A4}$$

According to Eqs. (A3) and (A4), the stiffness of the bulk substrate could be obtained as

$$k_\mathrm{b} = \frac{\mathrm{d}F}{\mathrm{d}\delta_\mathrm{b}} = \frac{4}{3} r_\mathrm{b} E_\mathrm{b} \tag{A5}$$

As shown in Eq. (A1), k_a is not a constant value but a function of δ_a, and the value of δ_a should be determined in advance to obtain the equivalent stiffness. The following two equations could be used on basis of the elastic compatibility conditions (Yeo et al. 2009):

$$F = k \times \delta = k_\mathrm{a} \times \delta_\mathrm{a} = k_\mathrm{b} \times \delta_\mathrm{b} \tag{A6}$$

$$\delta = \delta_\mathrm{a} + \delta_\mathrm{b} \tag{A7}$$

Applying Eqs. (A1) and (A5)–(A6) and (A7), δ_a is related to δ by

$$\frac{3\sqrt{\rho} E_\mathrm{a}}{2 r_\mathrm{b} E_\mathrm{b}} \delta_\mathrm{a}^{3/2} + \delta_\mathrm{a} - \delta = 0 \tag{A8}$$

Then, we can obtain

$$\delta_\mathrm{a} = \frac{\delta}{1 + \frac{3\sqrt{\rho} E_\mathrm{a}}{2 r_\mathrm{b} E_\mathrm{b}} \sqrt{\delta_\mathrm{a}}} \tag{A9}$$

As for rock joint, for simplicity, we can treat $E_\mathrm{a} = E_\mathrm{b}$, $\rho = r_\mathrm{b}$.

Equation (A9) is a iterative equation and can be solved numerically by the fixed point iteration method (Yeo et al. 2009). Therefore, after two iterations, an approximate solution for the asperity deformation could be given by:

$$\delta_\mathrm{a} = \frac{\delta}{1 + \frac{3}{2\sqrt{\rho}} \sqrt{\delta \Big/ \left(1 + \frac{3}{2\sqrt{\rho}} \sqrt{\delta/2}\right)}} \tag{A10}$$

Equation (A10) is the asperity deformation which takes into account the bulk substrate deformation and is not equal to the applied displacement δ, but instead is given as a function of δ.

If we take into account the bulk substrate deformation, the asperity deformation δ_a is expressed as

$$\begin{aligned} \delta_\mathrm{a} &= g(\delta) = g(z-d) \\ &= \frac{(z-d)}{1 + \frac{3}{2\sqrt{\rho}} \sqrt{(z-d) \Big/ \left(1 + \frac{3}{2\sqrt{\rho}} \sqrt{(z-d)/2}\right)}} \end{aligned} \tag{A11}$$

Substituting Eq. (A11) into Brown model (Brown and Scholz 1985, 1986), the normal stress is given by

$$\sigma_\mathrm{n} = \frac{4}{3} E' \eta \sqrt{\rho} \int_d^\infty \sqrt{\{g[z-d]\}^3} f(z) \mathrm{d}z \tag{A12}$$

Rearrange Eq. (A12), we can obtain Eq. (10).

References

Baghbanan A, Jing LR (2007) Hydraulic properties of fractured rock masses with correlated fracture length and aperture. Int J Rock Mech Sci 44(5):704–719

Bandis S, Lumsden AC, Barton N (1983) Fundamental of rock joint deformation. Int J Rock Mech Sci Geomech Abstr 20(6):249–268

Barton NR, Bandis SC, Bakhtar K (1985) Strength, deformation and conductivity coupling of rock joints. Int J Rock Mech Min Sci Geomech Abstr 22(3):121–140

Bower KM, Zyvoloski G (1997) A numerical model for thermo-hydro-mechanical coupling in fractured rock. Int J Rock Mech Min Sci 34(8):1201–1211

Brown SR, Scholz CH (1985) Closure of random elastic surfaces in contact. J Geophys Res 90(B7):5531–5545

Brown SR, Scholz CH (1986) Closure of rock joints. J Geophys Res 91(B7):4939–4945

Cook NGW (1992) Natural joints in rock: mechanical, hydraulic and seismic behavior and properties under normal stress. Int J Rock Mech Sci Geomech Abstr 29(3):198–223

Goodman RE (1976) Methods of geological engineering in discontinuous rocks. West, New York

Greenwood J, Tripp JH (1970) The contact of two nominally flat rough surfaces. Proc Inst Mech Engrs 185(1):625–633

Greenwood JA, Williamson JBP (1966) Contact of nominally flat surfaces. Proc Roy Soc Lond 195(Ser A):300–319

Guvanasen V, Chan T (2000) A three-dimensional numerical model for thermohydromechanical deformation with hysteresis in a fractured rock mass. Int J Rock Mech Sci 37(1–2):89–106

Hopkins DL (2000) The implications of joint deformation in analyzing the properties and behavior of fractured rock masses, underground excavations, and faults. Int J Rock Mech Sci 37(1–2):175–202

ISRM (1978) Suggested methods for the quantitative description of discontinuities in rock masses. Int J Rock Mech Sci Geomech Abstr 15(6):319–368

Itasca Consulting Group (2004) Universal distinct element code (version 4.0) user's guide. Minneapolis

Lee SD, Harrison JP (2001) Empirical parameters for non-linear fracture stiffness from numerical experiments of fracture closure. Int J Rock Mech Sci 38(5):721–727

Malama B, Kulatilake PHSW (2003) Models for normal fracture deformation under compressive loading. Int J Rock Mech Sci 40(6):893–901

Marache A, Riss J, Gentier S (2008) Experimental and modeled mechanical behavior of a rock fracture under normal stress. Rock Mech Rock Eng 41:869–892

Popov VL (2010) Contact mechanics and friction: physical principles and applications. Springer, Berlin, Heidelberg

Swan G (1983) Determination of stiffness and other joint properties from roughness measurements. Rock Mech Rock Eng 16(1):19–38

Tao QF, Ghassemi A, Christine A et al (2011) A fully coupled method to model fracture permeability change in naturally fractured reservoirs. Int J Rock Mech Sci 48(2):259–268

Xia CC, Yue ZQ, Tham LG et al (2003) Quantifying topography and closure deformation of rock joints. Int J Rock Mech Sci 40(2):197–220

Xia CC, Wang W, Ding ZZ (2008) Development of three-dimensional TJXW-3D-typed portable rock surface topography. Chin J Rock Mech Eng 27:1502–1512 (in Chinese with english abstract)

Xia CC, Tang ZC, Xiao WM et al (2013) New peak shear strength criterion of rock joints based on quantified surface description. Rock Mech Rock Eng. doi:10.1007/s00603-013-0395-6

Yamada K, Takeda N, Kagami J et al (1978) Mechanisms of elastic contact and friction between rough surfaces. Wear 48(1):15–34
Yeo CD, Katta RR, Polycarpou AA (2009) Improved elastic contact model accounting for asperity and bulk substrate deformation. Tribol Lett 35:191–203
Zhao ZH, Jing LR, Neretnieks I et al (2011) Analytical solution of coupled stress-flow-transport processes in a single rock fracture. Comput Geosci 37:1439–1449